Effective Slip over Superhydrophobic Surfaces in Thin Channels

François Feuillebois,[1] Martin Z. Bazant,[1,2] and Olga I. Vinogradova[1,3]

[1]*CNRS UMR 7636 and 7083, ESPCI, 10 rue Vauquelin, 75005 Paris, France*
[2]*Departments of Chemical Engineering and Mathematics, Massachusetts Institute of Technology,
Cambridge, Massachusetts 02139, USA*
[3]*A. N. Frumkin Institute of Physical Chemistry and Electrochemistry, Russian Academy of Sciences,
31 Leninsky Prospect, 119991 Moscow, Russia*
(Received 2 August 2008; published 15 January 2009)

Superhydrophobic surfaces reduce drag by combining hydrophobicity and roughness to trap gas bubbles in a microscopic texture. Recent work has focused on specific cases, such as arrays of pillars or grooves, with limited theoretical guidance. Here, we consider the experimentally relevant limit of thin channels and obtain rigorous bounds on the effective slip length for any two-component (e.g., low-slip and high-slip) texture with given area fractions. Among all anisotropic textures, parallel stripes attain the largest (or smallest) possible slip in a straight, thin channel for parallel (or perpendicular) orientation with respect to the mean flow. Tighter bounds for isotropic textures further constrain the effective slip. These results provide a framework for the rational design of superhydrophobic surfaces.

Introduction.—The design and fabrication of micro and nanotextured surfaces have received much attention in recent years. In case of a hydrophobic texture, a modified surface profile leads to a very large contact angle and can induce novel properties, which could not be achieved without roughness [1]. Thus, the remarkable mobility of liquids on such superhydrophobic surfaces in the Cassie state, i.e., where the texture is filled with gas, renders them ''self-cleaning,'' and causes droplets to roll (rather than slide) under gravity and rebound (rather than spread) upon impact. Beyond their fundamental interest, such surfaces may impact microfluidics [2,3], by reducing viscous drag in very thin channels and amplifying transport phenomena [4] and transverse flows [5].

Reduced wall friction is associated with the breakdown of the no-slip hypothesis. It has recently become clear that liquid slippage occurs at smooth hydrophobic surfaces and can be described by the boundary condition [6–8], $v_s = b\partial v/\partial z$, where v_s is the (tangential) slip velocity at the wall, $\partial v/\partial z$ the local shear rate, and b the slip length, which can reach tens of nm [9]. A mechanism for large slippage involves a lubricating gas layer of thickness δ with viscosity μ_g much smaller than that of the liquid μ [10] so that $b \approx \delta(\mu/\mu_g - 1) \approx 50\delta$ [11]. Slip lengths up to tens of μm may be then obtained over a gas layer stabilized with a rough wall texture. The composite nature of the texture, however, requires regions of lower slip (or no slip) in direct contact with the liquid, so the effective slip length of the surface b^* (defined below) is reduced. For anisotropic textures, b^* depends on the flow direction and is generally a tensor [14]. Indeed, experimental studies of flow past superhydrophobic surfaces suggest that b^* does not exceed several μm [15] (except for a special design

[16]) and varies with the orientation of the wall texture relative to flow [17].

The quantitative understanding of liquid slippage past superhydrophobic surfaces is still challenging. Some exact solutions are known for a flow on alternating (parallel or transverse) no-slip and perfect-slip stripes [18,19] or transverse inhomogeneous slip sectors [20]. Simple scaling expressions have been proposed for a geometry of pillars [8,21], and numerical approaches have also been followed [22–24]. Nevertheless, general principles to maximize or minimize the effective slip have not yet been established, even in the simple (but experimentally relevant) lubrication limit, where the implication of slip is the most pronounced [10].

In this Letter, we propose a systematic approach to quantify and optimize the effective slip length in a thin channel. Rather than a precise discussion of the liquid flow past composite regions, we use the theory of transport in heterogeneous media [25,26], which provides exact results for an *effective permeability* over length scales much larger than the heterogeneity. From this theory, we derive rigorous bounds on an *effective slip length* for arbitrary anisotropic or isotropic textures, given only the area fraction and local (any) slip lengths of the high-slip and low-slip regions. These bounds constrain the attainable effective slip and provide theoretical guidance for texture optimization since they are attained only by certain special textures in the theory. In some regimes, the bounds are close enough to obviate the need for tedious calculations of flows over particular textures.

Model and analysis.—We consider pressure-driven flow of a viscous fluid between two textured parallel plates (''+'' and ''−'') separated by h, as sketched in Fig. 1.
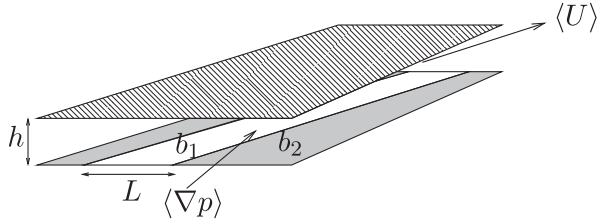
FIG. 1.   Sketch of a thin channel, where the gap width h is small compared with the texture characteristic length L.

Motivated by superhydrophobic surfaces in the Cassie state, we assume flat interfaces (as in most previous studies [18,22]) and corresponding to a minimum dissipation [19,27]) characterized by spatially varying, piecewise constant, slip lengths $b^+(x, y)$ and $b^-(x, y)$. Our analysis is based on the lubrication (or Hele-Shaw) limit of a thin channel, where the texture varies over a scale $L \gg h$; the flow profile is then locally parabolic in a domain where slip lengths are constant. To evaluate the effective slip length, we first integrate this parabolic velocity profile across the channel to obtain the depth-averaged velocity $\mathbf{U}$ in terms of the pressure gradient $\boldsymbol{\nabla} p$ along the plates. The result is an expression of Darcy's law,

$$\mathbf{U} = -\frac{k(x, y)}{\mu}\boldsymbol{\nabla} p, \qquad (1)$$

where we obtain the piecewise constant permeability

$$k(x, y) = \frac{h^2}{12}\left(1 + \frac{3(\beta^+ + \beta^- + 4\beta^+\beta^-)}{1 + \beta^+ + \beta^-}\right) \qquad (2)$$

in terms of the normalized slip lengths $\beta^+ = b^+(x, y)/h$ and $\beta^- = b^-(x, y)/h$. As usual in Hele-Shaw flow, we neglect localized flow perturbations around the jumps in $b^+(x, y)$ and $b^-(x, y)$. We consider case (I) of one no-slip wall ($\beta^+ = \beta(x, y)$; $\beta^- = 0$), which is relevant for various setups, where the alignment of opposite textures is inconvenient or difficult. Since the permeability (2) is maximized with two equal surfaces, $\beta^+ = \beta^- = \beta(x, y)$, we also consider this case (II) with the goal of minimizing drag [28]. The permeability then takes the form

$$k(x, y) = \frac{h^2}{12} \times \begin{cases} 1 + 3\beta(x, y)/[1 + \beta(x, y)] & \text{case (I)} \\ 1 + 6\beta(x, y) & \text{case (II)} \end{cases}.$$
$$(3)$$

The slip length can also vary with orientation and thus is generally a second-rank tensor $\mathbf{b}(x, y)$, from which a tensorial permeability $\mathbf{k}(x, y)$ can be derived [14].

The slip length $b(x, y)$ (or $\mathbf{b}(x, y)$) varies on the microscale $L \gg h$, but we are interested in properties of the flow at the macroscale. A natural definition of the effective slip length is based on a hypothetical uniform channel with the same effective permeability. First, we average (1) over the texture (denoted by $\langle.\rangle$) at a mesoscale that is smaller than the macroscale, but much larger than L, to obtain

$$\langle\mathbf{U}\rangle = -\frac{1}{\mu}\langle k(x, y)\boldsymbol{\nabla} p\rangle = -\frac{\mathbf{k}^*}{\mu}\cdot\langle\boldsymbol{\nabla} p\rangle$$

where in the last step, we introduce the effective permeability $\mathbf{k}^*$, which is generally a tensor, even if $k(x, y)$ is locally isotropic. Only with an isotropic structure at the mesoscale does it become a scalar k^*. This definition is subject to the boundary condition of a uniform pressure gradient $\boldsymbol{\nabla} P$ applied at the macroscale, which must equal the average pressure gradient, $\langle\boldsymbol{\nabla} p\rangle = \boldsymbol{\nabla} P$, since the pressure is harmonic [25].

By analogy with (3), we define the effective slip length in terms of the effective permeability:

$$k_j^* = \frac{h^2}{12} \times \begin{cases} 1 + 3\beta_j^*/[1 + \beta_j^*] & \text{case (I)} \\ 1 + 6\beta_j^* & \text{case (II)} \end{cases} \qquad (4)$$

where the principal (eigen) directions $j = 1, 2$ of $\mathbf{k}^*$ correspond with those of $\boldsymbol{\beta}^* = \mathbf{b}^*/h$, where $\mathbf{b}^*$ is the effective slip length tensor [14].

We then assume $b(x, y)$ switches between two values, b_1 and b_2, associated with permeabilities k_1, k_2 from (3), for regions (or "phases") of liquid-solid and liquid-gas interfaces, respectively. Let ϕ_1 and ϕ_2 be the area fractions of the two phases with $\phi_1 + \phi_2 = 1$. We make no further assumptions in deriving bounds on the effective slip length β^* in a principal direction (without transverse flow), aside from distinguishing between anisotropic and isotropic textures.

Anisotropic textures.—For any two-component texture, if only the fraction of each component is known, the so-called Wiener bounds apply [26]: $k^\perp \leq k^* \leq k^\parallel$, where k^* is an eigenvalue of $\mathbf{k}^*$. The lower bound $k^\perp = (\phi_1/k_1 + \phi_2/k_2)^{-1}$ is attained by parallel stripes perpendicular to the pressure gradient and the upper bound $k^\parallel = \phi_1 k_1 + \phi_2 k_2$ by stripes parallel the pressure gradient [Fig. 2(a)], which correspond to familiar limits of resistors in series or in parallel, respectively.

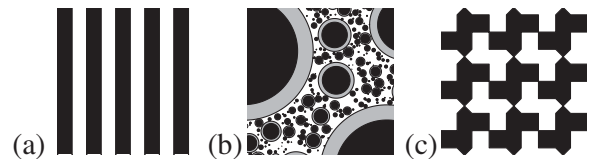Using (3) and (4), the corresponding bounds for the effective slip length are

FIG. 2.   Special textures arising in the theory: (a) stripes, which attain the Wiener bounds of maximal and minimal effective slip, if oriented parallel or perpendicular to the applied pressure gradient, respectively; (b) the Hashin-Shtrikman fractal pattern of nested circles, which attains the maximal/minimal slip among all isotropic textures (patches should fill up the whole space, but their number is limited here for clarity); and (c) the Schulgasser texture, whose effective slip follows from the phase-interchange theorem.

$$\frac{\langle\beta\rangle + 4\beta_1\beta_2}{1 + 4\langle\tilde{\beta}\rangle} \leq \beta^* \leq \frac{\langle\beta\rangle + \beta_1\beta_2}{1 + \langle\tilde{\beta}\rangle} \quad \text{case (I)} \quad \text{(5a)}$$

$$\frac{\langle\beta\rangle + 6\beta_1\beta_2}{1 + 6\langle\tilde{\beta}\rangle} \leq \beta^* \leq \langle\beta\rangle \quad \text{case (II)} \quad \text{(5b)}$$

where

$$\langle\beta\rangle = \phi_1\beta_1 + \phi_2\beta_2 \quad \text{and} \quad \langle\tilde{\beta}\rangle = \phi_2\beta_1 + \phi_1\beta_2 \quad (6)$$

are the average slip length and average transposed slip length, respectively. Using parameters for typical super-hydrophobic surfaces, these bounds are plotted versus the liquid-gas area fraction ϕ_2 in Fig. 3(a) and versus the liquid-gas slip length β_2 in Fig. 3(b). In case (I), the bounds are fairly close (especially when β_2 is large), so the theory provides a good sense of the possible effective slip of any texture, based only on the area fractions and local slip lengths. In case (II), the difference between the upper and lower bounds is larger and grows quickly with β_2.

Isotropic textures.—Consider now any isotropic structure, without a preferred direction ($\mathbf{k}^* = k^*\mathbf{I}$). If the only

(a)

(b)

FIG. 3. (a) Bounds on the (normalized) superhydrophobic slip length β^*/β_2 versus the liquid-gas area fraction ϕ_2, assuming no-slip $\beta_1 = 0$ and high-slip $\beta_2 = 5$ on the liquid-solid and liquid-gas interfaces, respectively. Bottom: zoom of top figure. Gray and black lines and symbols correspond to cases (I) and (II), that is one or two superhydrophobic surfaces, respectively. The solid lines represent the Wiener bounds and the dashed lines represent the HS bounds. The values of β^* for the chessboard or the isotropic Schulgasser structure are also shown as circles. (b) The same bounds plotted versus the slip length β_2 for $\phi_2 = 0.9$.

knowledge about the two-phase texture is ϕ_1, ϕ_2, then the Hashin-Shtrikman (HS) bounds apply for the effective permeability [26], $k_{\text{HS}}^L \leq k^* \leq k_{\text{HS}}^U$, where (assuming $\beta_1 \leq \beta_2$ without loss of generality)

$$k_{\text{HS}}^L = \langle k\rangle - \frac{\phi_1\phi_2[k]^2}{\langle\tilde{k}\rangle + k_1}, \qquad k_{\text{HS}}^U = \langle k\rangle - \frac{\phi_1\phi_2[k]^2}{\langle\tilde{k}\rangle + k_2}$$

with $[k] = k_2 - k_1$ and using the same notation as in (6). Each bound can be attained by the special HS fractal pattern [26] sketched in Fig. 2(b). For one bound, space is filled by disks of all sizes, each containing a circular core of one component and a thick ring of the other (with proportions set by the concentration), and switching the components gives the other bound. Fractal geometry is not necessary, however, since periodic honeycomblike structures can also attain the bounds [29].

Using (3) and (4), the corresponding bounds for the effective slip length are obtained in a form similar to (5)

$$\frac{\langle\beta\rangle + f(\beta_1)\beta_1\beta_2}{1 + f(\beta_1)\langle\tilde{\beta}\rangle} \leq \beta^* \leq \frac{\langle\beta\rangle + f(\beta_2)\beta_1\beta_2}{1 + f(\beta_2)\langle\tilde{\beta}\rangle} \quad (7)$$

where $f(\beta) = \begin{cases} (5 + 3\beta)/(2 + 5\beta) & \text{case (I)} \\ 3/(1 + 3\beta) & \text{case (II)} \end{cases}$. (8)

The HS bounds (7) are plotted in Fig. 3 in the same way as the Wiener bounds (5) and behave similarly, aside from being closer and confined between them. However, it turns out that isotropy does not dramatically reduce (enhance) the maximum (minimum) effective slip in a thin channel, especially in the configuration with two superhydrophobic surfaces, case (II).

Finally, we use phase-interchange results [26] to obtain the effective slip length without any calculations, for a special class of isotropic textures. For one that is invariant by a $\pi/2$ rotation followed by a phase interchange, a classical result follows: $k^* = \sqrt{k_1 k_2}$. Examples include the chessboard and the Schulgasser texture, sketched in Fig. 2(c). The effective β^* obtained from (4) is shown in Fig. 3(a). For case (I), it is close to the HS upper bound, although for case (II), it is not.

Design strategies.—We close by proposing some guidelines for the design of thin superhydrophobic microchannels, which maximize effective slippage, e.g., for lab-on-a-chip applications. We assume a principal direction of the texture is aligned with the side walls since this is typically the fastest orientation. (Tilted textures also complicate the analysis since the constraint of no transverse flow, $\langle U\rangle_y = 0$, induces a transverse pressure gradient, $\langle\boldsymbol{\nabla} p\rangle_y = -(k_{yx}^*/k_{yy}^*)\langle\boldsymbol{\nabla} p\rangle_x$, which in turn affects the mean forward flow, $\langle U\rangle_x = -(1/\mu)\det(\mathbf{k}^*)/k_{yy}^*$ [14].) For simplicity, we also restrict now to the case $\beta_1 = 0$ of no-slip support structures.

It has been predicted for thick ($L \ll h$) cylindrical [18] and planar channels [22] that the longitudinal stripe con-
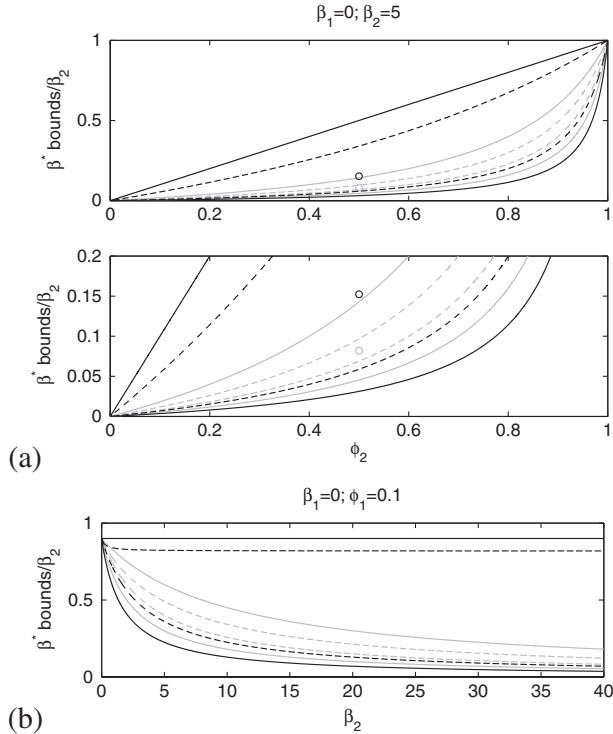
figuration has larger effective slip than the transverse one. For a thin channel ($L \gg h$), we can now draw the more general conclusion that longitudinal (transverse) stripes provide the largest (smallest) possible slip that can be achieved by any texture. Interestingly, this in contrast to a prediction for thick channels, where an array of pillars in the limit $\phi_2 \to 1$ has larger slip than longitudinal stripes [21].

We have shown that the key parameter determining effective slip is the area fraction of solid, ϕ_1, in contact with the liquid. If this is very small (or $\phi_2 \to 1$) for all textures, the effective slip tends to a maximum, $\beta^* \to \beta_2$. In this limit, the microchannel produces a kind of super-fluidity, with pluglike flow. However, even a very small ϕ_1 is enough to reduce the effective slip significantly since in this limit [except an upper limit for case (II), where $\phi_2 - \beta^*/\beta_2 = 0$] we have for case (I) the asymptotic scaling $\phi_2 - \beta^*/\beta_2 \propto \phi_1$. It is interesting that in case of perfect slip over the gas areas, β^* scales as $\propto \phi_2/\phi_1$, which is similar to an earlier result for a thick cylinder with transverse stripes [18]. For thin channels, we see now that this result is the very general upper bound, valid for any texture (and likely any channel geometry) with perfect slip patterns, representing "obstacles" to the flow. We conclude that in many situations, maximizing β_2 is not nearly as important as optimizing the texture to achieve large effective slip.

Finally, we have demonstrated that the largest possible β^* for any slip lengths or area fractions is equal to the area-averaged slip length $\langle\beta\rangle$, attained by longitudinal stripes [case (II)]. Optimal isotropic textures (e.g., honeycomb) exhibit smaller β^*, but may be preferable to enhance the stability of the gas-liquid interfaces. For all textures, the effective slip nearly coincides with the average, if β_2 is small (or $\beta_2 - \beta_1 \ll 1$). Although this limit is less important for pressure-driven microfluidics, it may have relevance for amplifying transport phenomena [4].

In summary, we have derived rigorous bounds on the effective slip of two-component textures in thin channels, which can guide the design of superhydrophobic surfaces for micro/nanofluidics, and some general principles may hold for thick channels as well.

[1] D. Quere, Rep. Prog. Phys. **68**, 2495 (2005).
[2] H. A. Stone, A. D. Strooock, and A. Ajdari, Annu. Rev. Fluid Mech. **36**, 381 (2004).
[3] T. M. Squires and S. R. Quake, Rev. Mod. Phys. **77**, 977 (2005).
[4] A. Ajdari and L. Bocquet, Phys. Rev. Lett. **96**, 186102 (2006).
[5] A. D. Stroock, S. K. W. Dertinger, A. Ajdari, I. Mezíc, H. A. Stone, and G. M. Whitesides, Science **295**, 647 (2002).
[6] O. I. Vinogradova, Int. J. Miner. Process. **56**, 31 (1999).
[7] E. Lauga, M. P. Brenner, and H. A. Stone, *Handbook of Experimental Fluid Dynamics* (Springer, NY, 2007), Chap. 19, pp. 1219–1240.
[8] L. Bocquet and J. L. Barrat, Soft Matter **3**, 685 (2007).
[9] O. I. Vinogradova and G. E. Yakubov, Langmuir **19**, 1227 (2003).
[10] O. I. Vinogradova, Langmuir **11**, 2213 (1995).
[11] A variant of this picture is a nanobubble-coated hydro-phobic surface [12,13].
[12] O. I. Vinogradova, N. F. Bunkin, N. V. Churaev, O. A. Kiseleva, and B. W. Ninham, J. Colloid Interface Sci. **173**, 443 (1995).
[13] B. M. Borkent, S. M. Dammler, H. Schönherr, G. J. Vansco, and D. Lohse, Phys. Rev. Lett. **98**, 204502 (2007).
[14] M. Z. Bazant and O. I. Vinogradova, J. Fluid Mech. **613**, 125 (2008).
[15] P. Joseph, C. Cottin-Bizonne, J. M. Benoit, C. Ybert, C. Journet, P. Tabeling, and L. Bocquet, Phys. Rev. Lett. **97**, 156104 (2006).
[16] C. Lee, C. H. Choi, and C. J. Kim, Phys. Rev. Lett. **101**, 064501 (2008).
[17] J. Ou and J. P. Rothstein, Phys. Fluids **17**, 103606 (2005).
[18] E. Lauga and H. A. Stone, J. Fluid Mech. **489**, 55 (2003).
[19] M. Sbragaglia and A. Prosperetti, Phys. Fluids **19**, 043603 (2007).
[20] A. A. Alexeyev and O. I. Vinogradova, Colloids Surfaces A **108**, 173 (1996).
[21] C. Ybert, C. Barentin, C. Cottin-Bizonne, P. Joseph, and L. Bocquet, Phys. Fluids **19**, 123601 (2007).
[22] C. Cottin-Bizonne, C. Barentin, E. Charlaix, L. Bocquet, and J. L. Barrat, Eur. Phys. J. E **15**, 427 (2004).
[23] R. Benzi, L. Biferale, M. Sbragaglia, S. Succi, and F. Toschi, J. Fluid Mech. **548**, 257 (2006).
[24] N. V. Priezjev, A. A. Darhuber, and S. M. Troian, Phys. Rev. E **71**, 041608 (2005).
[25] K. Z. Markov, in *Heterogeneous Media, Modelling and Simulation*, edited by K. Markov and L. Preziosi (Birkhauser, Boston, 2000), Chap. 1, pp. 1–162.
[26] S. Torquato, *Random Heterogeneous Materials: Microstructure and Macroscopic Properties* (Springer, New York, 2002).
[27] J. Hyväluoma and J. Harting, Phys. Rev. Lett. **100**, 246001 (2008).
[28] Stability issues are not considered here, but note that in case (II), one can expect dewetting in a very thin channel so that a relevant experimental situation is likely only that of $h \geq 1$ μm [G. E. Yakubov, H.-J. Butt, and O. I. Vinogradova, J. Phys. Chem. B **104**, 3407 (2000)]. Case (I) may then be preferred for smaller channel thickness.
[29] S. Torquato, L. Gibiansky, M. Silva, and L. Gibson, Int. J. Mech. Sci. **40**, 71 (1998).